1. PanNiobium

Thermodynamic database for multi-component
Nb-rich alloys

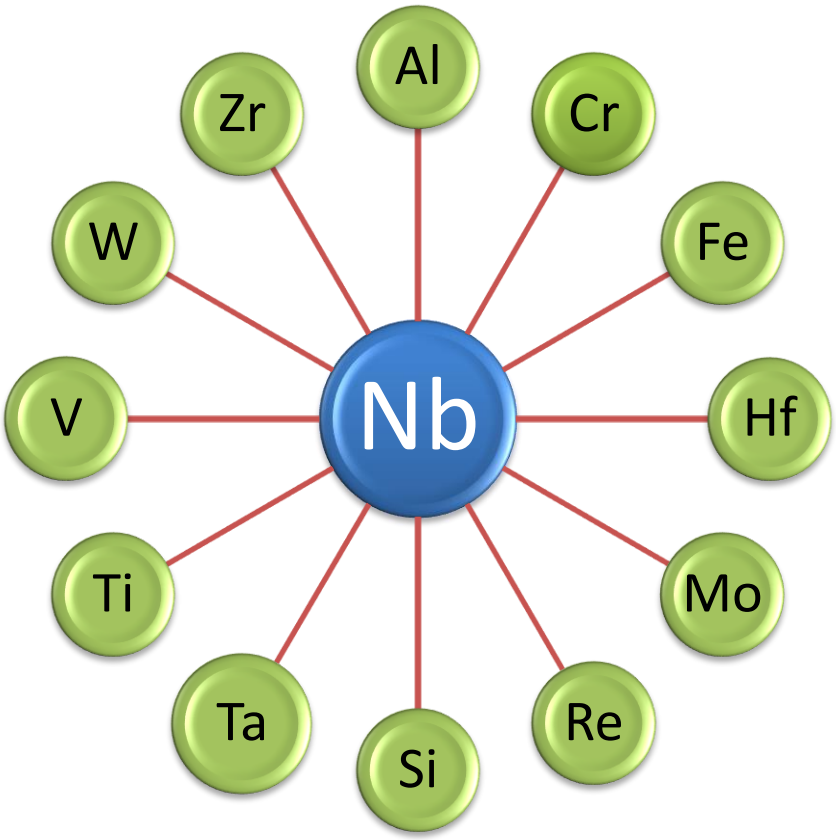

Copyright © CompuTherm LLC

1.1 Components

Total of 13 components are included in the database as listed here:

Al, Cr, Fe, Hf, Mo, **Nb**, Re, Si, Ta,Ti, V, W, and Zr

1.2 Suggested Composition Range

The suggested composition range for each element is listed in Table 1.1. It should be noted that this given composition range is rather conservative. It is derived from the chemistries of the multicomponent commercial alloys that have been used to validate the current database. In the subsystems, many of these elements can be applied to a much wider composition range.

Table 1.1: Suggested composition range

Element	Composition range (at.%)
Nb	50 ~ 100
Si, Ti	0 ~ 30
Cr	0 ~ 20
Al, Hf, V	0 ~ 10
Fe, Mo, Ta, Re, W, Zr	0 ~ 5

1.3 Phases

Total of 131 phases are included in the database and a few key phases are listed in Table 1.2. Information on all phases can be displayed in the TDB viewer of Pandat or can be found at www.computherm.com.

Table 1.2: Phase name and related information

Name	Lattice Size	Constituent
A15_Nb3Al	(0.75)(0.25)	(Cr,Fe,Hf,Mo,Nb,Si,Ti,V)(Al,Cr,Nb,Si,Ti,V)
Al12Mo	(12)(1)	(Al)(Mo)
Al17Mo4	(17)(4)	(Al)(Mo)
Al22Mo5	(22)(5)	(Al)(Mo)

Al5Mo	(5)(1)	(Al)(Mo)
Al63Mo37	(63)(37)	(Al)(Mo)
Al69Ta39	(0.6389)(0.3611)	(Al,Ta)(Al,Ta)
AlMo3	(1)(3)	(Al,Mo)(Al,Mo)
Bcc	(1)(3)	(Al,Cr,Fe,Hf,Mo,Nb,Re,Si,Ta,Ti,V,W,Zr)(Va)
Chi_A12	(24)(10)(24)	(Cr,Fe,Re)(Cr,Mo,Nb,Re,Ta,Ti,W,Zr)(Cr,Fe,Mo,Nb,Re,Ta,W)
DO22	(0.25)(0.75)	(Al,Cr,Nb,Ti)(Al,Cr,Si,Ti)
Fcc	(1)(1)	(Al,Cr,Fe,Hf,Mo,Nb,Re,Si,Ta,Ti,V,W,Zr)(Va)
Hcp	(1)(0.5)	(Al,Cr,Fe,Hf,Mo,Nb,Re,Si,Ta,Ti,V,W,Zr)(Va)
Laves_C14	(2)(1)	(Al,Cr,Fe,Hf,Mo,Nb,Re,Si,Ta,Ti,V,Zr)(Al,Cr,Fe,Hf,Mo,Nb,Re,Ta,Ti,V,W,Zr)
Laves_C15	(2)(1)	(Al,Cr,Hf,Mo,Nb,Ta,Ti,V,W,Zr)(Al,Cr,Hf,Mo,Nb,Ta,Ti,V,W,Zr)
Mo4Si9Ti7	(0.55)(0.45)	(Mo,Ti)(Si)
Mu_Phase	(1)(2)(4)(6)	(Fe,Mo,Nb,Ta,W)(Fe,Mo,Nb,Ta,W)(Fe,Mo,Nb,Ta,Ti,W)(Fe,Mo,Ta,W)
Nb5Si3	(0.625)(0.375)	(Cr,Hf,Nb,Ti,V,Zr)(Al,Si)
Sigma	(8)(4)(18)	(Al,Fe,Re,Si,Ta,Ti)(Cr,Fe,Mo,Nb,Ta,V,W)(Al,Cr,Fe,Mo,Nb,Re,Si,Ta,Ti,V,W)

1.4 Key Elements and Subsystems

The modeling status for the constituent binaries and ternaries are given in Table 1.3 and Table 1.4. The color represents the following meaning:

: Full description

: Full description for major phases

: Extrapolation

Table 1.3: Current modeling status for all the constituent binary systems

	Cr	Fe	Hf	Mo	Nb	Re	Si	Ta	Ti	V	W	Zr
Al												
Cr												
Fe												
Hf												
Mo												
Nb												
Re												
Si												
Ta												
Ti												
V												
W												

Table 1.4: Current modeling status for all the constituent ternary systems

Al-Nb-Ti	Cr-Fe-Si	Cr-Hf-Si	Cr-Nb-Si	Cr-Nb-Ti	Cr-Nb-V	Cr-Nb-Zr	Cr-Si-Ti
Cr-Si-V	Cr-Ti-Zr	Fe-Nb-Ti	Hf-Nb-Si	Hf-Nb-Zr	Hf-Si-Ti	Mo-Nb-Re	Mo-Nb-W
Mo-Si-Ti	Nb-Re-Zr	Nb-Si-Ti	Nb-Si-W	Nb-Ta-Zr	Re-Ti-Zr	Ta-Ti-Zr	Ta-V-W

1.5 Database Validation

The current PanNb database was validated by large amounts of phase equilibrium data available for Nb alloys. A few examples are given here. Figure 1.1 shows the calculated liquidus projection of Nb-Ti-Si together with the experimental data [1997Bew]. The different symbol of experimental data denotes that the primary solidification phase observed in the as-cast microstructure of the alloy. The two invariant reactions at the metal-rich region of Nb-Ti-Si are $L+Nb_5Si_3 \rightarrow Ti_5Si_3+Nb_3Si$ at 1599°C and $L+Nb_3Si \rightarrow Ti_5Si_3+Bcc$ at 1359°C.

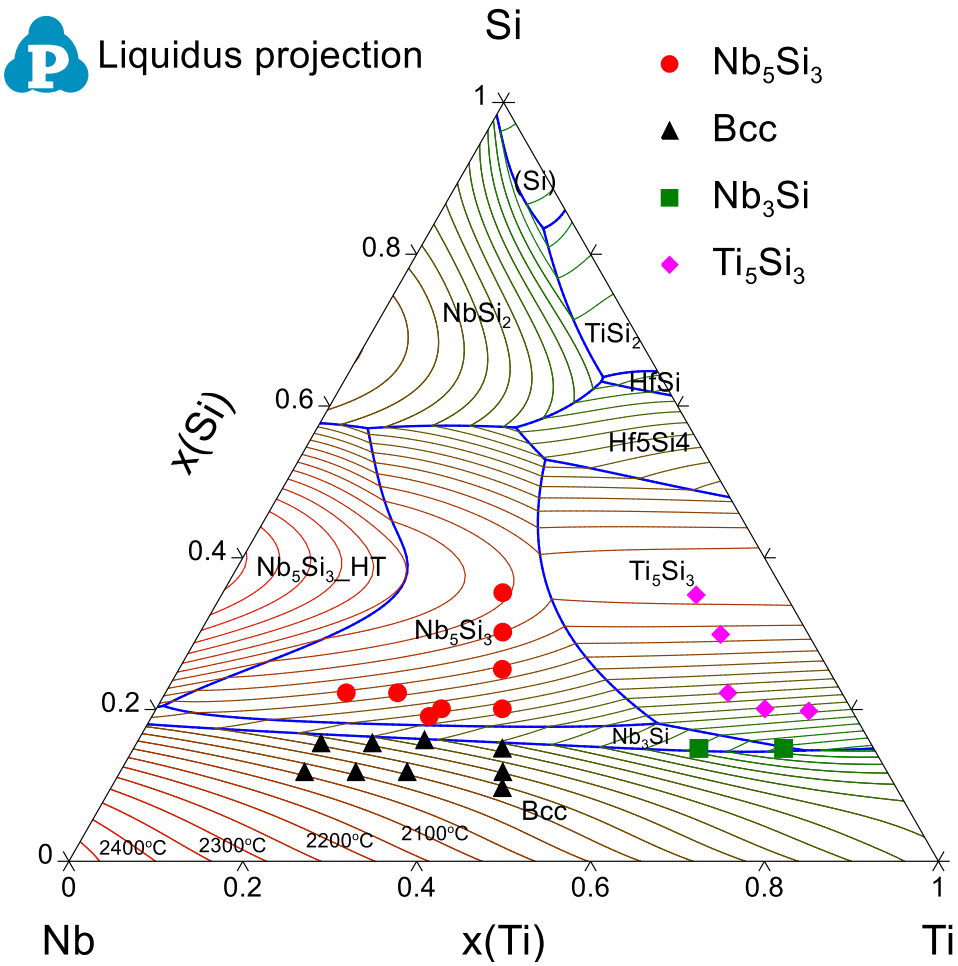

Figure 1.1: Calculated liquidus projection of Nb-Ti-Si together with experimental data [1997Bew]

Figure 1.2 and Figure 1.3 show the calculated isothermal section of Nb-Ti-Si at 1500°C and 1340°C, respectively. The experimental data are also plotted for comparison. The phase compositions are from EPMA measurements. The detail of experiments can be found in literature [1998Bew]. Different shapes of the symbols denote the different phase regions where the alloys are located. The green lines are tie lines.

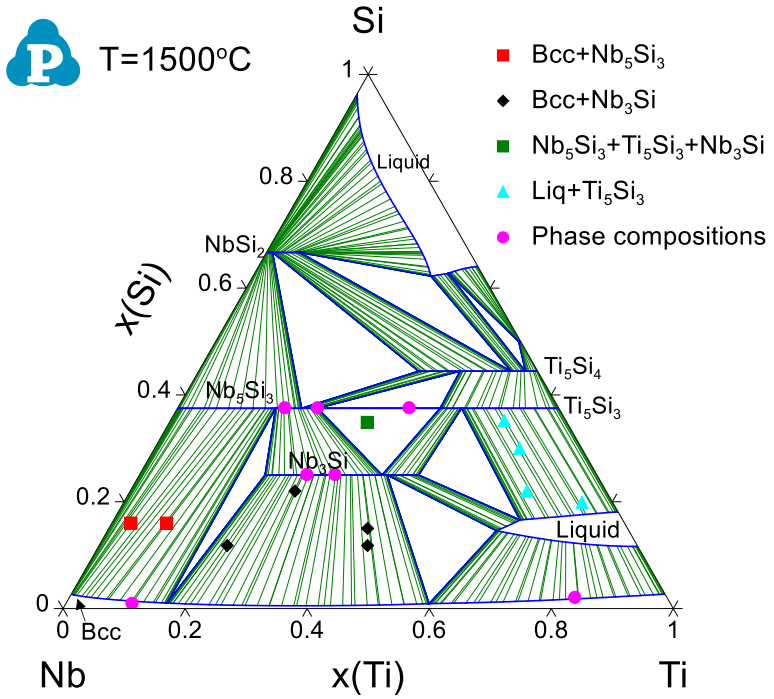

Figure 1.2: Calculated isothermal section of Nb-Ti-Si at 1500°C together with experimental data [1998Bew]

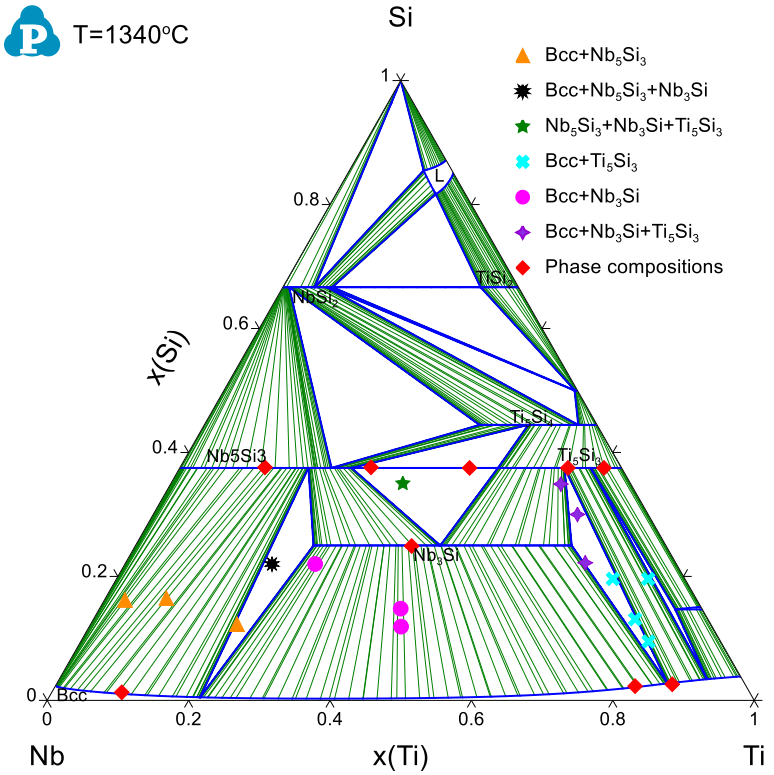

Figure 1.3: Calculated isothermal section of Nb-Ti-Si at 1340°C together with experimental data [1998Bew]

Figure 1.4 shows the calculated liquidus projection of Nb-Cr-Si overlaid by experimental data. Again, the different symbol of experimental data [2007Bew] denotes that the primary solidification phase observed in the as-cast microstructure of the alloy. Figure 1.5 shows the calculated isothermal section of Nb-Cr-Si at 1100°C. In PanNb, a ternary phase $Nb_9Si_2Cr_3$, was included in the thermodynamic description of the Nb-Cr-Si system for the first time.

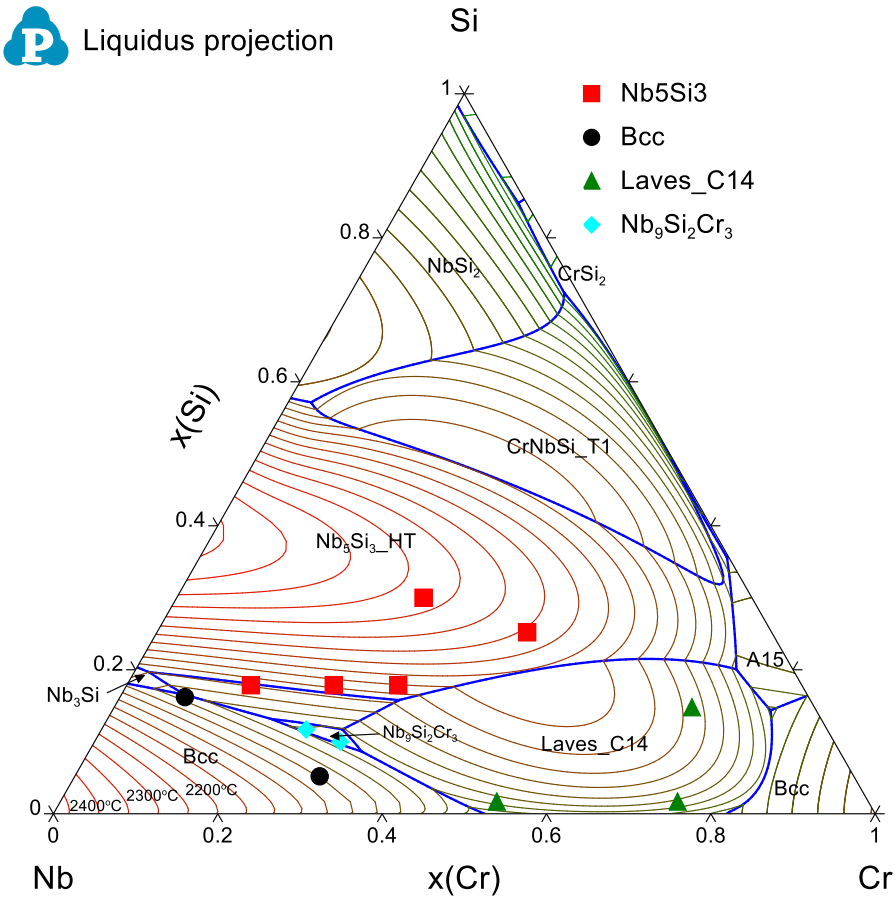

Figure 1.4: Calculated liquidus projection of Nb-Cr-Si together with experimental data [2007Bew, 2009Bew]

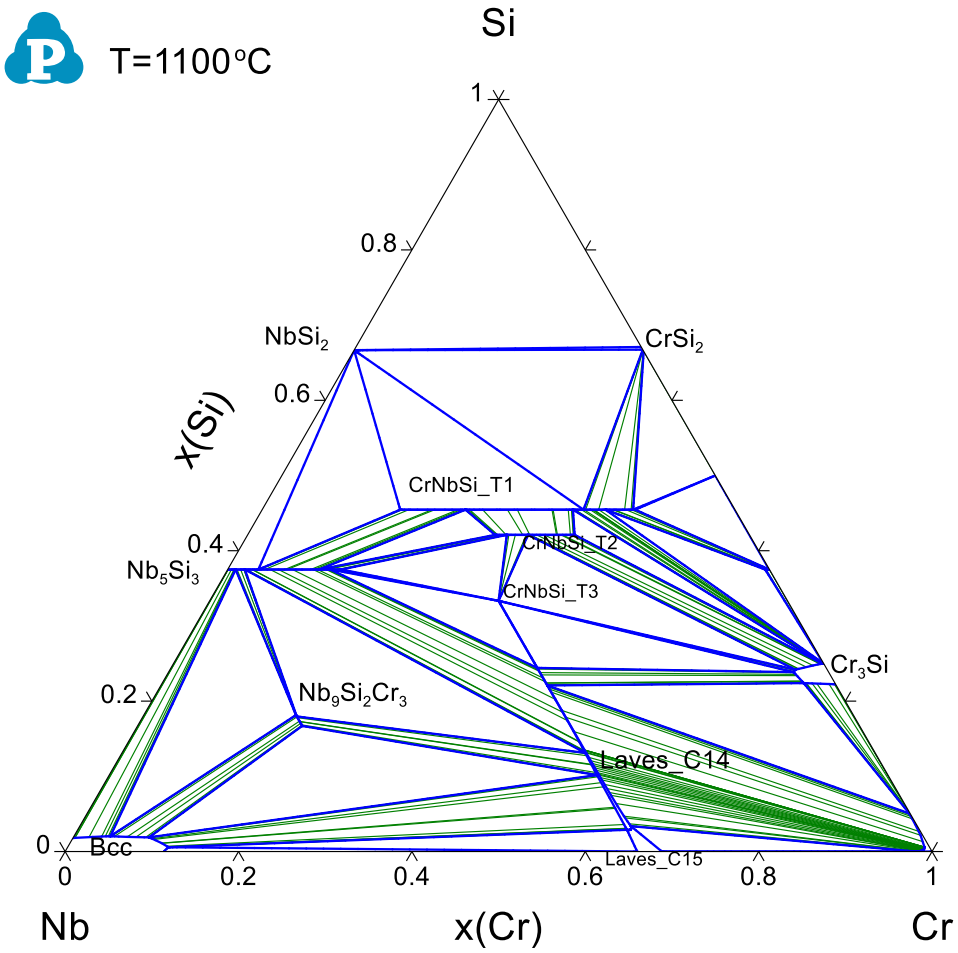

Figure 1.5: Calculated isothermal section of Nb-Cr-Si at 1100°C

Figure 1.6 shows the calculated liquidus projection of the Nb-Si-Hf overlaid by experimental data [1999Bew]. Again, the different symbol of experimental data denotes that the primary solidification phase observed in the as-cast microstructure of each alloy. The three invariant reactions at the metal-rich region of Nb-Hf-Si are L+Hf_5Si_3→Nb_5Si_3_LT+Hf_2Si at 2035°C, L+Nb_3Si→ Nb_5Si_3_LT + Bcc at 1836°C and L+Nb_5Si_3_LT→Hf_2Si + Bcc at 1822°C. Figure 1.7 shows the calculated isothermal section of Nb-Hf-Si at 1500°C together with experimental data.

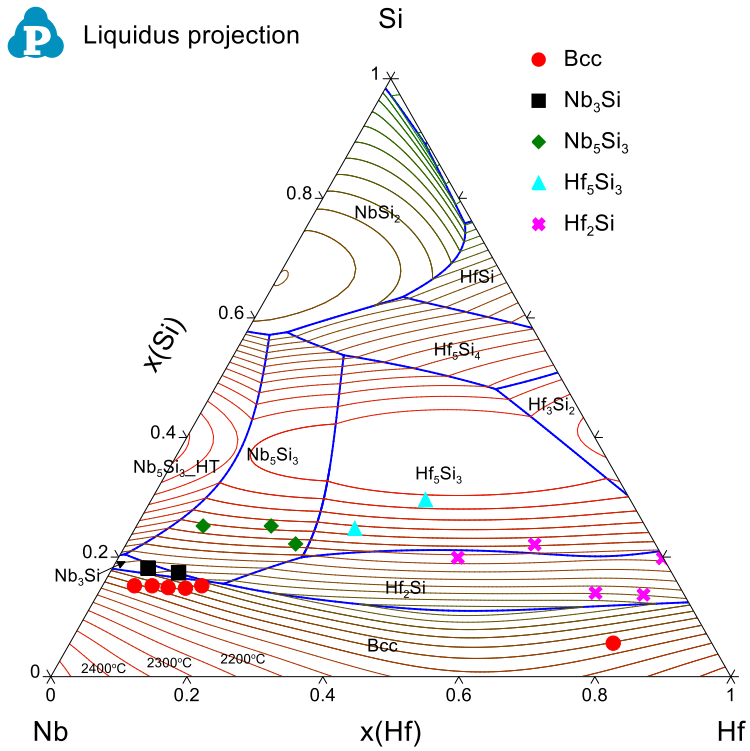

Figure 1.6: Calculated liquidus projection of Nb-Hf-Si together with experimental data [1999Bew, 2003Yan]

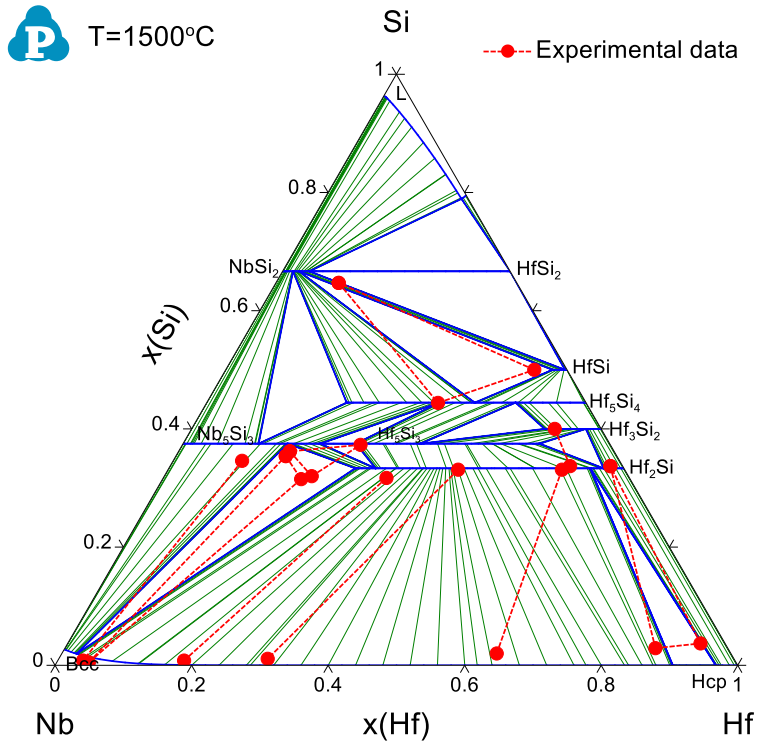

Figure 1.7: Calculated isothermal section of Nb-Hf-Si at 1500°C together with experimental data [2001Zha]

Comparisons between the calculated phase compositions (in italic font) and the EPMA measurements for two Nb-Cr-Ti-Si alloys are shown in Table 1.5. These measured phase compositions were not used in model parameter optimization. Instead, they were only used for validation of the calculated results. In view of this, the calculated phase compositions from the current thermodynamic description agree well with the experimental measurements. However, the users should be cautious on the discrepancy between the calculated and measured Cr and Nb compositions for the Laves_C14 phase.

Table 1.5: Comparisons between the EMPA measured and the calculated (italic font in parentheses) phase compositions [2003Yan]

Sample	Phase	Nb (at.%)	Cr (at.%)	Ti (at.%)	Si (at.%)
Nb-10Cr-23Ti-15Si	Bcc_a2	58.2 (*60.9*)	13.3 (*11.9*)	27.4 (*26.1*)	1.2 (*1.1*)
	Nb_5Si_3	42.2 (*41.5*)	0.6 (*1.5*)	21.2 (*19.5*)	36.1 (*37.5*)
	Laves_C14	29.1 (*21.9*)	47.1 (*55.5*)	14.7 (12.7)	9 (*9.9*)
Nb-11Cr-23Ti-13Si	Bcc_a2	59.4 (*61.2*)	13.5 (*12.0*)	26 (*25.7*)	1.2 (*1.1*)
	Nb_5Si_3	43.7 (*41.6*)	0.5 (*1.6*)	19.5 (*19.3*)	36.2 (*37.5*)
	Laves_C14	26 (*22.1*)	51 (*55.5*)	13 (*12.5*)	10 (*9.9*)

Figure 1.8(a)-(b) show the simulated solidification paths for the Nb-11Cr-23Ti-13Si, and Nb-21Cr-23.5Ti-15.5Si alloys. The BSE images of the as-cast microstructures of these two alloys are shown in Figure 1.8(c)-(d), respectively. The phase observed in the BSE images is well predicted by the lever-rule simulation and the early stage of the Scheil simulation. The additional phases predicted by the Scheil model were not identified in the BSE images, which maybe either due to the small amount presented in the microstructure or the micro-segregation in real cooling condition is not as severe as assumed by Scheil simulation.

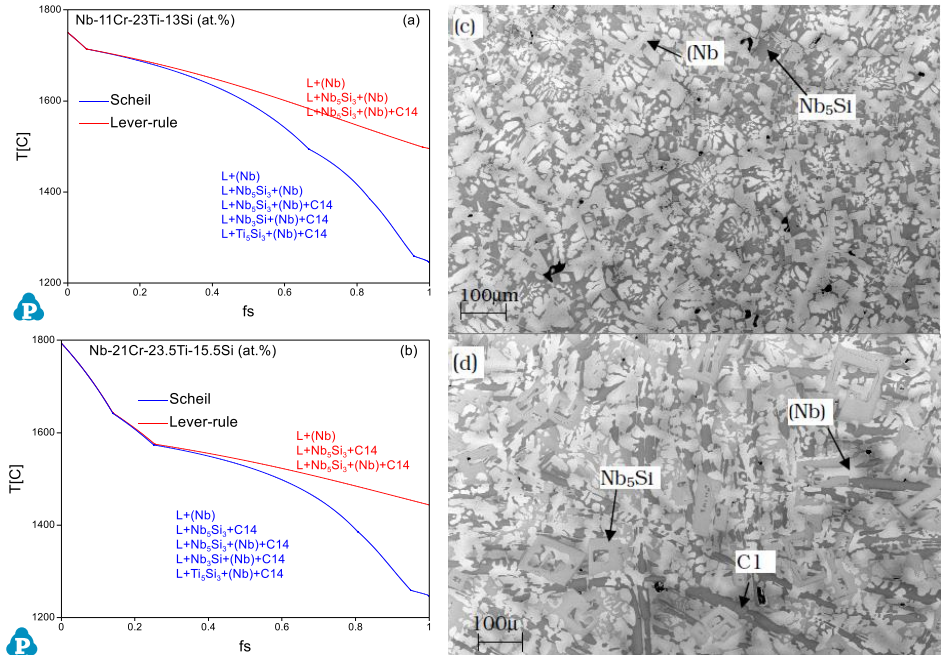

Figure 1.8: Calculated solidification paths with experimental observation (a) and (c) for alloy Nb-11Cr-23Ti-13Si; (b) and (d) for alloy Nb-21Cr-23.5Ti-15.5Si

Figure 1.9 (a) and (b) show the solidification path simulations under the Scheil and lever-rule condition for the six component Nb-22Ti-2Hf-4Cr-3Al-16Si alloy, and the BSE image of the as-cast microstructure of the same alloy. The microstructure consists of two phases (Nb) and Nb_5Si_3, which is well predicted by the lever-rule simulation as shown by the dash line in Figure 1.9 (a). The Scheil simulation predicted the formation of Ti_5Si_3 and Laves_C14 in addition to (Nb) and Nb_5Si_3. However, the total mole percentage of Ti_5Si_3 and Laves_C14 is predicted to be less than 5%. Again, the additional phases predicted by the Scheil model were not identified in the BSE images, which maybe either due to the small amount presented in the microstructure or the micro-segregation in real cooling condition is not as severe as assumed by Scheil simulation.

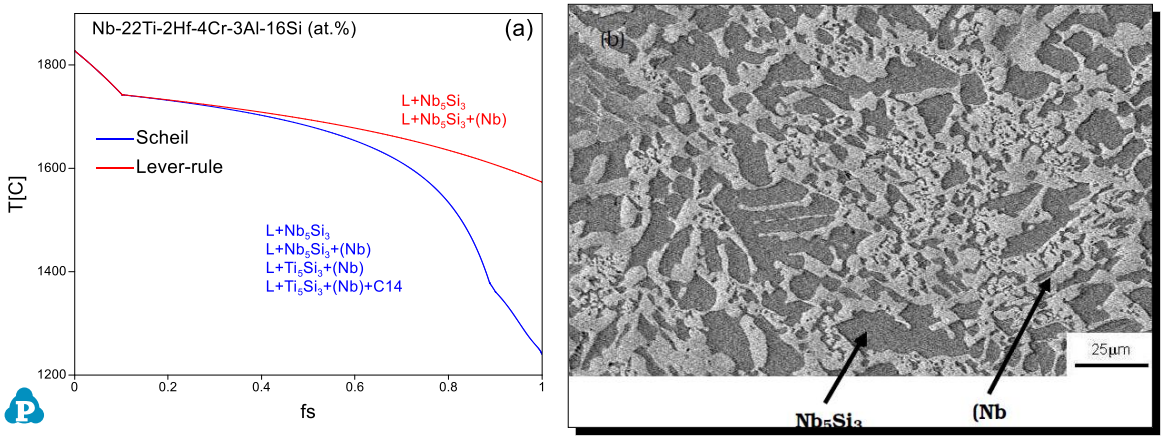

Figure 1.9: Calculated solidification path for alloys Nb-22Ti-2Hf-4Cr-3Al-16Si with experimental observation

1.6 References

[1997Bew] B. P. Bewlay, M. R. Jackson, H. A. Lipsitt, Journal of Phase Equilibria, 18(3)(1997): 264-278.

[1998Bew] B. P.Bewlay, M. R. Jackson, R. R. Bishop, Journal of Phase Equilibria, 19(6) (1998): 577-586.

[2007Bew] B. Bewlay, P.; Y. Yang, R. L. Casey, M. R. Jackson, Y. A. Chang, Materials Research Society Symposium Proceedings, 980 (2007): 333-338.

[2009Bew] B.P. Bewlay, Y. Yang, R. L. Caesy, M.R. Jackson Y. A. Chang, Intermetallics, 17(3) (2009): 120-127.

[1999Bew] B.P. Bewlay, R.R. Bishop, M.R.Jackson, Zeitschrift fuer Metallkunde, 90(6) (1999): 413-422.

[2003Yan] Y. Yang,Y. A. Chang, J.-C. Zhao, B.P. Bewlay, Intermetallics: 11(5) (2003): 407-415.

[2001Zha] J.-C. Zhao, B.P. Bewlay, M.R.Jackson, Intermetallics, 9(8) (2001): 681-689.